small NANO MICRO

Graphene Oxide

Nanocomposites of Graphene Oxide and Upconversion Rare-Earth Nanocrystals with Superior Optical Limiting Performance

Wei Wei, Tingchao He, Xue Teng, Shixin Wu, Lin Ma, Hua Zhang, Jan Ma, Yanhui Yang, Hongyu Chen, Yu Han, Handong Sun, and Ling Huang**

***U**pconversion rare-earth nanomaterials (URENs) possess highly efficient near-infrared (NIR), e.g., 980 nm, laser absorption and unique energy upconversion capabilities. On the other hand, graphene and its derivatives, such as graphene oxide (GO), show excellent performance in optical limiting (OL); however, the wavelengths of currently used lasers for OL studies mainly focus on either 532 or 1064 nm. To design new-generation OL materials working at other optical regions, such as the NIR, a novel nanocomposites, GO–URENs, which combines the advantages of both its components, is synthesized by a one-step chemical reaction. Transmission electron microscopy, X-ray diffraction, infrared spectroscopy, and fluorescence studies prove that the α-phase URENs uniformly attach on the GO surface via covalent chemical bonding, which assures highly efficient energy transfer between URENs and GO, and also accounts for the significantly improved OL performance compared to either GO or URENs. The superior OL effect is also observed in the proof-of-concept thin-film product, suggesting immediate applications in making high-performance laser-protecting products and optoelectronic devices.*

W. Wei, X. Teng, Prof. Y. Yang, Prof. L. Huang
School of Chemical and Biomedical Engineering
Nanyang Technological University
70 Nanyang Drive, Singapore 637457
E-mail: LHuang@ntu.edu.sg
website: http://www.ntu.edu.sg/home/lhuang/

Dr. T. He, L. Ma, Prof. H. Chen, Prof. H. Sun
School of Physical and Mathematical Sciences
Nanyang Technological University
21 Nanyang Link, Singapore 637371
E-mail: hdsun@ntu.edu.sg

Dr. S. Wu, Prof. H. Zhang, Prof. J. Ma
School of Materials Science and Engineering
Nanyang Technological University
50 Nanyang Avenue
Singapore 639798

Prof. Y. Han
Chemical and Biological Engineering
King Abdullah University of Science and Technology
Thuwal 23955-6900, Kingdom of Saudi Arabia

DOI: 10.1002/smll.201200065

1. Introduction

Graphene has recently attracted dramatic interest from researchers working in physics, chemistry, biology, materials, and modeling, due to its superior mechanical, optical, and electronic properties, as well as its excellent controllability and manipulability compared to its analogues.[1–4] A large number of graphene-based applications in the areas of sensors, solar cells, transistors, and biochips have been developed.[5–7] However, graphene possesses large conjugated aromatic systems composed of sp^2-hybridized single-layer carbon atoms, and its hydrophobicity has rendered serious challenges for processing in aqueous media. A simple alteration is to oxidize graphene into graphene oxide (GO), which has become a well-adopted precursor to make various graphene-based nanomaterials.[8,9] For example, gold nanoparticles, quantum dots, and TiO_2 nanoparticles have been successfully decorated onto GO sheets.[10–12]

Due to the ultrafast carrier dynamics and the good incident light absorption capabilities, graphene and its derivatives

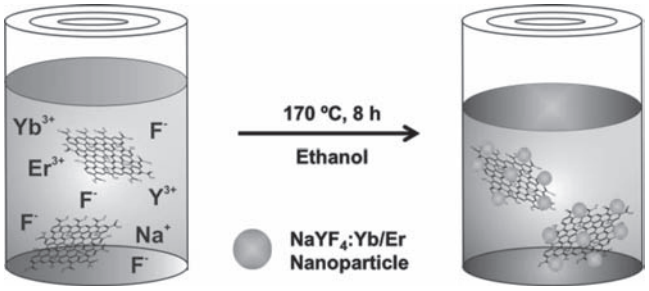

Scheme 1. Schematic illustration of the reaction for GO–UREN nanocomposite synthesis.

have become the benchmark standards for optical limiting (OL) studies.[13,14] With the principal structure of graphene reserved after oxidation, that is, the large conjugated aromatic system, GO and GO-based nanocomposites are also reported as decent candidates for broadband OL applications.[15,16] However, the current OL studies using graphene or GO mainly focus on the 532 or 1064 nm laser. Therefore, it is necessary to extend the laser working wavelength to other regions, such as the NIR, to broaden its applicability.

On the other hand, upconversion rare-earth nanomaterials (URENs) have shown strong NIR absorption and unique energy upconversion capabilities due to the special configuration of the 4f electrons in rare-earth elements. As a typical example, $NaYF_4$:Yb/Er nanoparticles can emit fluorescent visible light at high efficiency under NIR excitation,[17–19] thereby giving great potential in bioimaging, bioassay, and disease diagnosis.[17–21] However, studies on the nanocomposites of URENs and GO, which generates superior OL performance at the NIR region (e.g., 980 nm) by combining the advantages of both nanomaterials, are still absent. Herein, we report a facile method to synthesize GO–UREN nanocomposites (**Scheme 1**). Its superior OL performance under femtosecond 980 nm laser excitation is investigated, followed by demonstration of the mechanism study and proof-of-concept applications.

Scheme 1 depicts the experimental principles we employed to synthesize GO–UREN nanocomposites. Briefly, GO[10] was mixed with rare-earth elements in ethanol at a certain ratio, and the reaction was carried out in an autoclave at 170 °C for 8 h. Based on previous reports,[22,23] URENs are expected to be anchored onto the GO surface via the coordination interaction between rare-earth ions on URENs and carboxylic acid groups on GO. The short distance defined by the covalent bond assures that the fluorescence energy upconverted by URENs can be effectively transferred to GO, which is the foundation of our design of these nanocomposites for superior OL performance as discussed below.

2. Results and Discussion

The transmission electron microscopy (TEM) image in **Figure 1**a shows the synthesized nanocomposites of GO and $NaYF_4$:Yb/Er nanocrystals (abbreviated as GO–$NaYF_4$:Yb/Er). The $NaYF_4$:Yb/Er nanocrystals with sizes between 17 and 35 nm were anchored on a GO sheet (the dashed line indicates the contour of multiple pieces of GO). It is worth

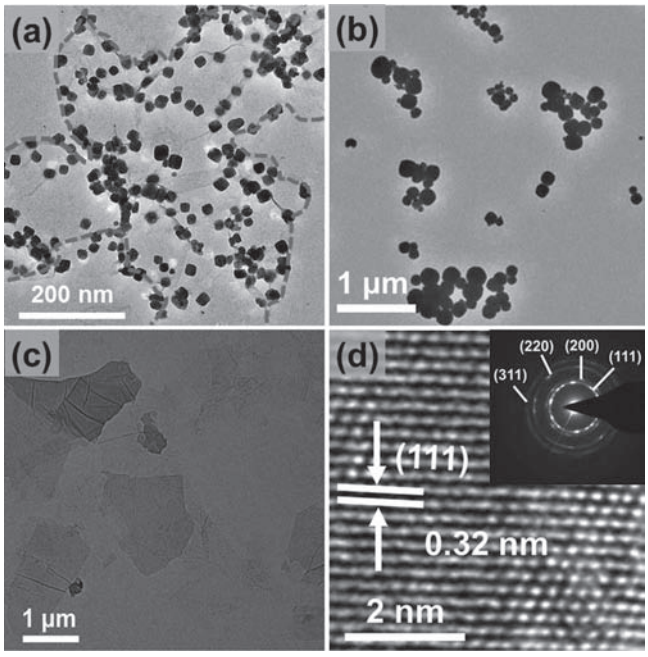

Figure 1. TEM images of a) GO–$NaYF_4$:Yb/Er, b) $NaYF_4$:Yb/Er nanoparticles, and c) GO. d) HRTEM image of $NaYF_4$:Yb/Er nanocrystals on GO. Inset: SAED pattern of $NaYF_4$:Yb/Er nanocrystal on GO.

noting that the $NaYF_4$:Yb/Er nanocrystals on GO look quite different from those synthesized under the same conditions but in the absence of GO (abbreviated as $NaYF_4$:Yb/Er nanoparticles), shown in Figure 1b, which are spherical particles with large size-distribution ranging from 30 to 200 nm. This difference is because here GO works not only as a substrate for $NaYF_4$:Yb/Er nanocrystal binding, but also behaves as a surfactant to regulate the growth of $NaYF_4$:Yb/Er nanocrystals via the -COOH and -OH groups,[12,24] which results in more uniform $NaYF_4$:Yb/Er nanocrystals than without GO. Figure 1c shows the TEM image of GO used for synthesizing the nanocomposites. The high-resolution TEM (HRTEM) image in Figure 1d reveals the α-phase structure of $NaYF_4$:Yb/Er nanocrystals on the GO surface, which agrees well with its cubic shape as can be seen in Figure 1a. The 0.32 nm lattice fringes corresponding to the (111) lattice plane also indicate that the nanocrystals are in the α phase. The selected area electron diffraction (SAED) pattern in Figure 1d suggests a polycrystalline structure of $NaYF_4$:Yb/Er nanocrystals, and the concentric rings indexed as the (111), (200), (220), and (311) planes of α-$NaYF_4$ are consistent with its X-ray diffraction (XRD) patterns, as shown in **Figure 2**a.

In Figure 2a, it is clear that GO–$NaYF_4$:Yb/Er contains XRD signals of both GO (Figure 2b) and a standard sample of α-phase $NaYF_4$ (JCPDS 06-0342, Figure 2c). In other words, the nanocomposites retains the crystal structures of both GO and $NaYF_4$:Yb/Er nanocrystals, and thus their principal properties and respective functionalities are also expected to be retained. Here we would like to emphasize that the characteristic XRD peaks of the $NaYF_4$:Yb/Er nanoparticles (Figure S1, Supporting Information, SI) are identical to those of both the standard sample (Figure 2c) and the $NaYF_4$:Yb/Er nanocrystals on the GO surface (Figure 2a).

small NANO MICRO

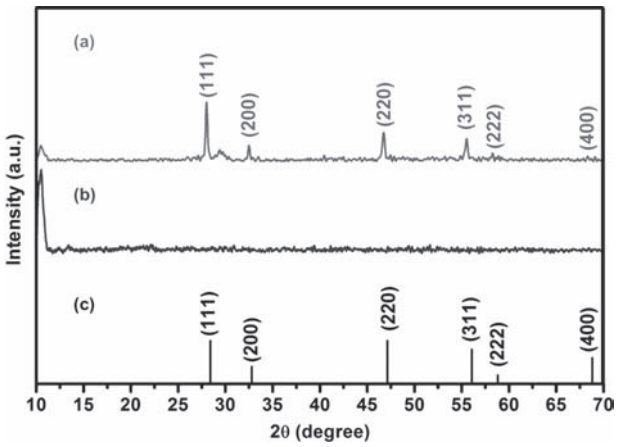

Figure 2. XRD patterns of a) GO–$NaYF_4$:Yb/Er, b) GO, and c) the standard sample of α-phase $NaYF_4$ (JCPDS 06-0342).

Comparison of the IR spectra provides more details on the interaction mode between $NaYF_4$:Yb/Er nanocrystals and the GO substrate in their nanocomposites. The peaks at 3421 (ν_{O-H}), 1733 ($\nu_{C=O}$), and 1629 cm^{-1} ($\nu_{C=C}$) in **Figure 3**c are the characteristics of the carboxyl and hydroxyl groups in GO generated by oxidation, while the peaks at 2924 and 2853 cm^{-1} can be assigned to the methylene stretching of CH_2 and CH moieties in GO. However, in Figure 3a, the weakened peak at 1733 cm^{-1} ($\nu_{C=O}$) implies the coordination interaction between the carboxyl groups on GO and the rare-earth ions on $NaYF_4$:Yb/Er nanocrystals, while the disappearance of the 1629 cm^{-1} peak further proves that the big aromatic system in GO was affected by this coordination interaction, which results in a new peak at 1595 cm^{-1} in the nanocomposites (Figure 3a) and also suggests the chemical interactions between $NaYF_4$:Yb/Er nanocrystals and GO.[22,23] The strong peak at 3460 cm^{-1} (ν_{O-H}) in Figure 3b comes from the water molecules adsorbed on $NaYF_4$:Yb/Er nanoparticles and the peak at 567 cm^{-1} represents the typical Ln–F (Ln = Y, Yb, Er) stretching vibration.[17–19,25]

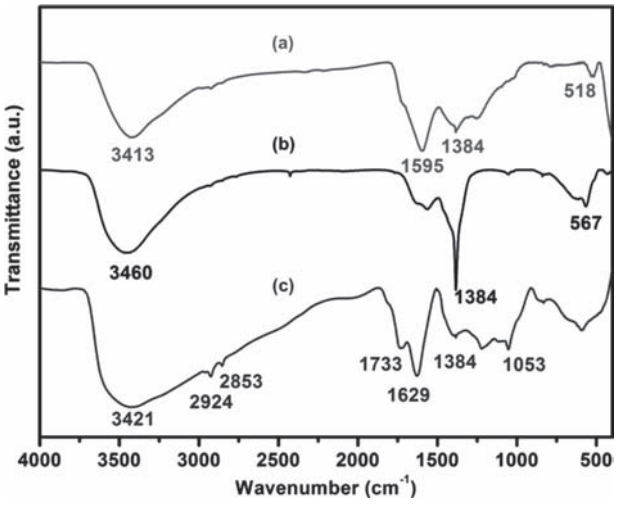

Figure 3. IR spectra of a) GO–$NaYF_4$:Yb/Er, b) $NaYF_4$:Yb/Er nanoparticles, and c) GO.

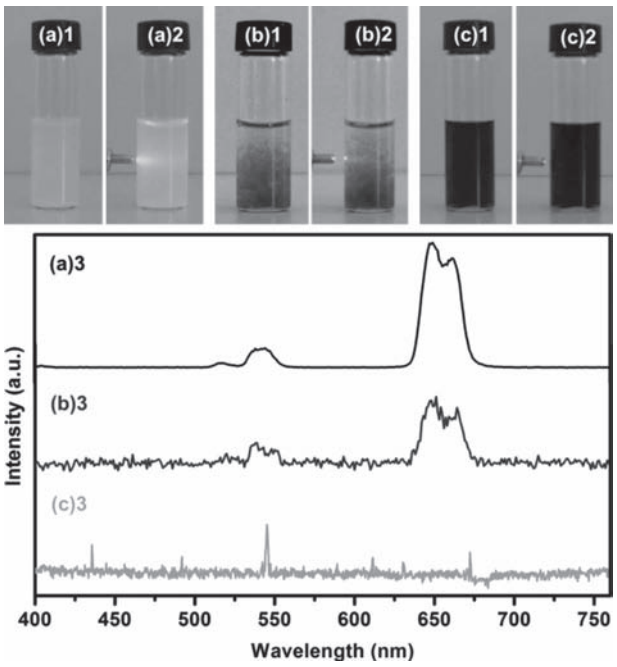

Figure 4. Photo images of a) $NaYF_4$:Yb/Er nanoparticles, b) physical mixture of $NaYF_4$:Yb/Er nanoparticles and GO, and c) GO–$NaYF_4$:Yb/Er in water/ethanol (1:1, v/v) solution before (a1, b1, c1) and after (a2, b2, c2) 980 nm laser excitation. a3, b3, and c3 are the upconversion fluorescence spectra of a2, b2, and c2 samples, respectively.

To study the energy transfer process between $NaYF_4$:Yb/Er nanocrystals and GO, we first characterized the upconversion fluorescence of $NaYF_4$:Yb/Er nanoparticles synthesized without GO. **Figure 4**a1 shows a solution of $NaYF_4$:Yb/Er nanoparticles in water/ethanol (1:1, v/v), and the opaque suspension indicates its poor solubility. However, under 980 nm laser excitation (Figure 4a2), a strong yellow light shows up. This proves that strong upconversion fluorescence was generated in $NaYF_4$:Yb/Er nanoparticles (note: the 980 nm laser is invisible to the naked eye), which can be further confirmed by the strong fluorescence spectrum (Figure 4a3) of the solution where three characteristic emission peaks at 510, 540, and 650 nm are observed.

In the case of GO–$NaYF_4$:Yb/Er, although it can form very uniform and stable solutions (Figure 4c1), there is no observable emission under laser excitation, as shown in Figure 4c2. The strong noise signal in Figure 4c3 clearly indicates that the upconverted fluorescence from $NaYF_4$:Yb/Er nanocrystals was completely quenched by GO, which otherwise would give the same spectrum as that of Figure 4b3. This is reasonable because GO has strong absorption at a broad wavelength range between 200 and 800 nm (Figure S2, SI), which covers the fluorescence emissions of $NaYF_4$:Yb/Er nanocrystals at 510, 540, and 650 nm; that is, the excitation energy of $NaYF_4$:Yb/Er nanocrystals falls within the absorption band of GO, so the upconverted energy from $NaYF_4$:Yb/Er nanocrystals can be effectively transferred to GO via the fluorescence resonance energy transfer (FRET) and/or the charge transfer (CT) mechanism.[21,26–29] As previously reported,[26–29] in order for the

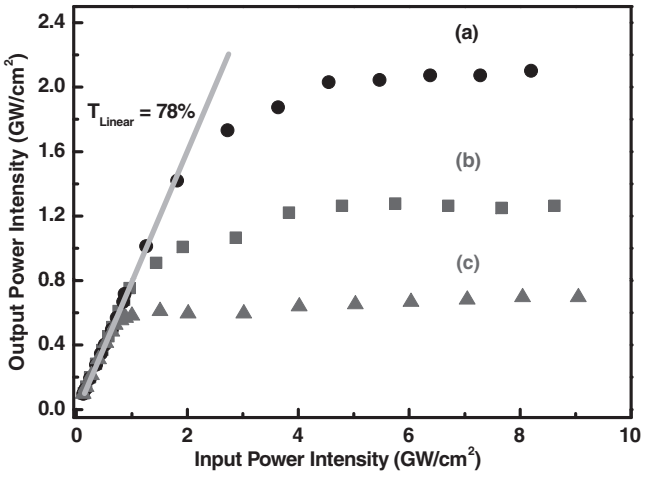

Figure 5. OL data for a) $NaYF_4$:Yb/Er nanoparticles, b) GO, and c) GO–$NaYF_4$:Yb/Er. All data were collected in water/ethanol (1:1, v/v) solution at 78% transmittance and under femtosecond 980 nm laser excitation.

energy transfer to happen at this high efficiency, the donor and the acceptor must be covalently connected, that is, the $NaYF_4$:Yb/Er nanocrystals must be chemically anchored on the GO substrate.

In a control experiment, we physically mixed $NaYF_4$:Yb/Er nanoparticles with GO in water/ethanol (1:1, v/v). The precipitate in Figure 4b1 indicates its poor stability. However, under excitation, a weak reddish color observed in Figure 4b2 proves the existence of the upconversion fluorescence, which is consistent with the fluorescence spectrum shown in Figure 4b3. This means the upconverted fluorescence from $NaYF_4$:Yb/Er nanoparticles is not completely, if at all, quenched by GO in the physical mixture. Actually, due to the large dynamic temporal distance between the $NaYF_4$:Yb/Er nanoparticles and the GO in solution, the quenching could hardly happen,[29] or at very low efficiency (<20%).[26] Instead, we conclude that the signal in Figure 4b3 becomes weaker than that in Figure 4a3 is mainly due to the scattering effect caused by the suspended GO pieces: a large portion of the laser energy is scattered away and only a small amount is responsible for the upconversion excitation. In other words, the structural difference between GO–$NaYF_4$:Yb/Er and the physical mixture of the components resulted in a significantly different fluorescence quenching efficiency.

Based on the results discussed above, an improved OL effect should be expected from GO–$NaYF_4$:Yb/Er compared to that of either $NaYF_4$:Yb/Er nanoparticles or GO at the NIR region. Indeed, the $NaYF_4$:Yb/Er nanoparticles give the poorest OL response (**Figure 5**a), which is due to the relatively small nonlinear scattering cross section, nonlinear absorption, and/or thermal lensing-induced nonlinear refraction of the nanoparticles.[30] In Figure 5b, GO shows 43% lower output power intensity than the $NaYF_4$:Yb/Er nanoparticles. This is reasonable because even though the large conjugated aromatic system was broken in GO during the oxidation process; the main skeleton and thus the ultrafast carrier and high light absorption capabilities of graphene are still retained, which assures the outstanding OL performance in GO.[14,15,31] More importantly, in GO–$NaYF_4$:Yb/Er, the chemical bond allows efficient energy transfer between $NaYF_4$:Yb/Er nanocrystals and GO, which results in significantly improved OL performance (Figure 5c) where 70 and 50% decreases of output power intensity were observed compared to those of $NaYF_4$:Yb/Er nanoparticles and GO, respectively. This means the chemically anchored $NaYF_4$:Yb/Er nanocrystals helped to double the OL performance of GO.

We believe this superior OL performance in GO–$NaYF_4$:Yb/Er arises from the following three factors. 1) The close distance defined by the chemical bond between $NaYF_4$:Yb/Er nanocrystals and GO substrate assures highly efficient energy transfer.[22,23] 2) The donor ($NaYF_4$:Yb/Er nanocrystals), which absorbs the NIR laser energy and upconverts into the visible fluorescence (Figure 4a3) at high efficiency, transfers the upconverted energy to the acceptor (GO) through nonradiative dipole–dipole coupling.[26–29,32] As depicted in **Figure 6**, the electrons in Yb^{3+} are first excited from $^2F_{7/2}$ to $^2F_{5/2}$ energy level, and then the excited electrons relax to the ground state by means of either energy transfer to Er^{3+} or radiation. The energy transferred to Er^{3+} further induces the electron excitation of $^4I_{15/2} \rightarrow {}^4I_{11/2}$, $^4I_{11/2} \rightarrow {}^4F_{7/2}$, as well as other multiphoton processes in Er^{3+}. Subsequently, Er^{3+} transfers its energy to the nearby GO via the FRET and/or CT process instead of the normal nonradiative relaxation of $^2H_{11/2} \rightarrow {}^4I_{15/2}$, $^4S_{3/2} \rightarrow {}^4I_{15/2}$, and $^4F_{9/2} \rightarrow {}^4I_{15/2}$, as we observed in Figure 4a3. This also explains why the fluorescence emission can be observed in the solution of $NaYF_4$:Yb/Er nanoparticles (Figure 4a2) as well as in its mixture with GO (Figure 4b2), but not in the nanocomposites (Figure 4c2). 3) The energy is further transferred into solution from the GO interface, which generates a large

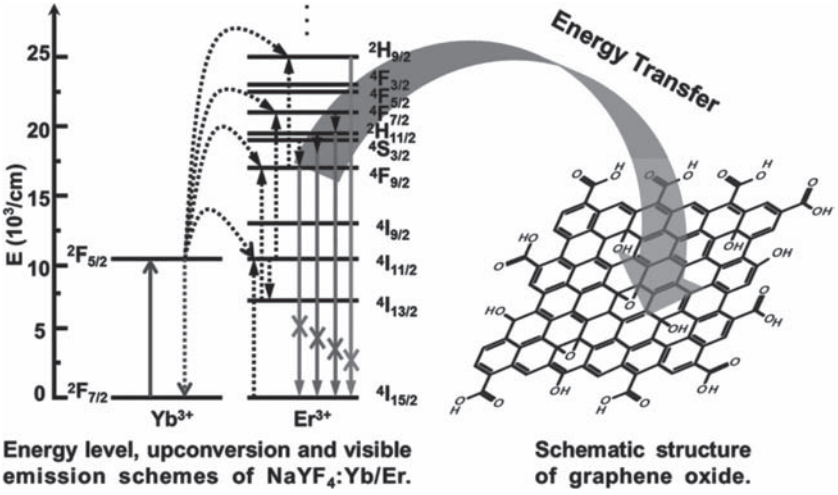

Figure 6. Scheme showing the energy upconversion mechanism of $NaYF_4$:Yb/Er nanocrystals (left), and the energy transfer process from $NaYF_4$:Yb/Er nanocrystals to GO (right).

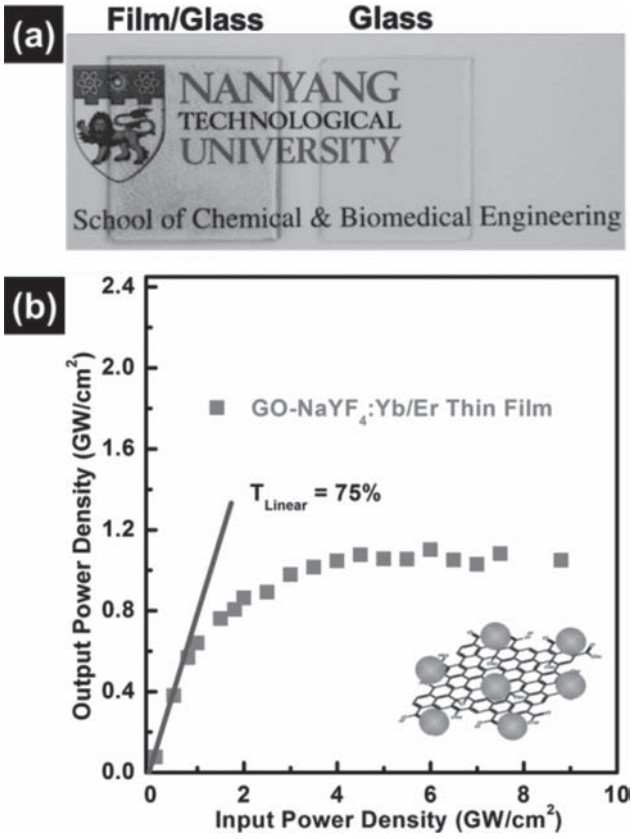

Figure 7. a) Photo images showing the transparency of glass slides with and without a coating of thin film composed of GO–$NaYF_4$:Yb/Er dispersed in PMMA (molecular weight: 22 000). b) OL performance of the nanocomposite–PMMA thin film coated on a glass slide. Inset: schematic structure of the GO–$NaYF_4$:Yb/Er nanocomposites.

quantity of bubbles (induced by thermal energy) at high efficiency due to the large surface area of GO. These bubbles usually cause strong nonlinear scattering effect (Figure S3, SI), which is responsible for the drastic decrease of the output energy.[31,32]

To prove the wide applicability of our concept for this nanocomposite design, we further synthesized the GO–$NaYF_4$:Yb/Tm nanocomposites, which has shown the same dramatically improved OL effect (Figure S4, SI) as that of GO–$NaYF_4$:Yb/Er. For the physical mixture of $NaYF_4$:Yb/Er nanoparticles and GO (Figure 4b1), the OL performance cannot be measured because of the serious scattering and/or reflection generated by the suspended GO.

We further fabricated a proof-of-concept product by coating a thin film of the GO–$NaYF_4$:Yb/Er nanocomposites dispersed in poly(methyl methacrylate) (PMMA) matrix (PMMA/nanocomposites, 97.5:2.5, w/w) on a glass slide.[15] It can be seen in **Figure 7**a that the glass slide coated with thin film shows a high transparency comparable to that without the film coating. Figure 7b indicates that this ~7.5-μm-thick film (Figure S5, SI) can generate an even better OL effect than the GO in solution with 10 mm optical length (Figure 5b), which suggests immediate applications in fabricating high-performance optical products.

3. Conclusion

In summary, we have developed a one-step facile method to synthesize novel GO–UREN nanocomposites that combine the advantages of both GO and URENs in the OL effect. The chemical interaction between GO and URENs assures highly efficient energy transfer within, and sequentially superior OL performance of, the nanocomposites. This study has not only broadened the working wavelengths of laser used for OL, from visible light to the NIR region, but also proved potential applications in the fabrication of lightweight, high-performance, laser-protecting products or optoelectronics.

Supporting Information

Supporting Information is available from the Wiley Online Library or from the author.

Acknowledgements

This work was supported by the Academic Research Fund (Tier 1) from Singapore Ministry of Education (RG 20/09) and the Start-Up Grant (SUG) from Nanyang Technological University. H.Z. is grateful for the support from MOE under AcRF Tier 2 (ARC 10/10, No. MOE2010-T2-1-060), Singapore National Research Foundation under the CREATE program: Nanomaterials for Energy and Water Management, and NTU under the New Initiative Fund FY 2010 (M58120031) in Singapore.

[1] T. Taychatanapat, K. Watanabe, T. Taniguchi, P. Jarillo-Herrero, *Nat. Phys.* **2011**, *7*, 621–625.
[2] X. Huang, X. Y. Qi, F. Boey, H. Zhang, *Chem. Soc. Rev.* **2012**,*41*, 666–686.
[3] X. Huang, Z. Y. Yin, S. X. Wu, X. Y. Qi, Q. Y. He, Q. C. Zhang, Q. Y. Yan, F. Boey, H. Zhang, *Small* **2011**,*7*, 1876–1902.
[4] J. T. Paci, T. Belytschko, G. C. Schatz, *J. Phys. Chem. C* **2007**, *111*, 18099–18111.
[5] T. Cohen-Karni, Q. Qing, Q. Li, C. M. Lieber, *Nano Lett.* **2010**, *10*, 1098–1102.
[6] V. C. Tung, J. Kim, L. J. Cote, J. Huang, *J. Am. Chem. Soc.* **2011**, *133*, 9262–9264.
[7] M. Arif, H. Kwang, B. Y. Lee, J. Lee, D. H. Seo, S. Seo, J. Jian, S. Hong, *Nanotechnology* **2011**, *22*, 355709/1–7.
[8] X. Huang, S. Z. Li, S. X. Wu, Y. Z. Huang, F. Boey, C. L. Gan, H. Zhang, *Adv. Mater.* **2012**, *24*, 979–983.
[9] X. Huang, X. Z. Zhou, S. X. Wu, Y. Y. Wei, X. Y. Qi, J. Zhang, F. Boey, H. Zhang, *Small* **2010**, *6*, 513–516.
[10] X. Z. Zhou, X. Huang, X. Y. Qi, S. X. Wu, C. Xue, F. Y. C. Boey, Q. Y. Yan, P. Chen, H. Zhang, *J. Phys. Chem. C* **2009**, *113*, 10842–10846.
[11] Y. Wang, H.-B. Yao, X.-H. Wang, S.-H. Yu, *J. Mater. Chem.* **2011**, *21*, 562–566.
[12] Y.-J. Xu, Y. Zhuang, X. Fu, *J. Phys. Chem. C* **2010**, *114*, 2669–2676.
[13] R. R. Nair, P. Blake, A. N. Grigorenko, K. S. Novoselov, T. J. Booth, T. Stauber, N. M. R. Peres, A. K. Geim, *Science* **2008**, *320*, 1308–1308.

[14] M. Breusing, C. Ropers, T. Elsaesser, *Phys. Rev. Lett.* **2009**, *102*, 086809/1–4.
[15] J. Balapanuru, J.-X. Yang, S. Xiao, Q. Bao, M. Jahan, L. Polavarapu, J. Wei, Q.-H. Xu, K. P. Loh, *Angew. Chem. Int. Ed.* **2010**, *49*, 6549–6553.
[16] G.-K. Lim, Z.-L. Chen, J. Clark, R. G. S. Goh, W.-H. Ng, H.-W. Tan, R. H. Friend, P. K. H. Ho, L.-L. Chua, *Nat. Photonics* **2011**, *5*, 554–560.
[17] M. Haase, H. Schäfer, *Angew. Chem. Int. Ed.* **2011**, *50*, 5808–5829.
[18] F. Wang, X. Liu, *Chem. Soc. Rev.* **2009**, *38*, 976–989.
[19] Z.-G. Yan, C.-H. Yan, *J. Mater. Chem.* **2008**, *18*, 5046–5059.
[20] J. Zhou, L. Yao, C. Li, F. Li, *J. Mater. Chem.* **2010**, *20*, 8078–8085.
[21] L. Y. Wang, R. X. Yan, Z. Y. Hao, L. Wang, J. H. Zheng, H. Bao, X. Wang, Q. Peng, Y. D. Li, *Angew. Chem. Int. Ed.* **2005**, *44*, 6054–6057.
[22] X. Zhang, X. Yang, Y. Ma, Y. Huang, Y. Chen, *J. Nanosci. Nanotechnol.* **2010**, *10*, 2984–2987.
[23] J. Guo, S. Zhu, Z. Chen, Y. Li, Z. Yu, Q. Liu, J. Li, C. Feng, D. Zhang, *Ultrason. Sonochem.* **2011**, *18*, 1082–1090.
[24] J. Kim, L. J. Cote, F. Kim, W. Yuang, K. R. Shull, J. Huang, *J. Am. Chem. Soc.* **2010**, *132*, 8080–8086.
[25] M. Fele-Beuermann, K. Lutar, Z. Mazej, S. Milicev, B. Zemva, *J. Fluorine Chem.* **1998**, *89*, 83–89.
[26] C. Liu, Z. Wang, H. Jia, Z. Li, *Chem. Commun.* **2011**, *47*, 4661–4663.
[27] X. Wu, H. Cao, B. Li, G. Yin, *Nanotechnology* **2011**, *22*, 075202/1–8.
[28] E. A. Jares-Erijman, T. M. Jovin, *Nat. Biotechnol.* **2003**, *21*, 1387–1395.
[29] M. Li, Q. Wang, X. Shi, L. A. Hornak, N. Wu, *Anal. Chem.* **2011**, *83*, 7061–7065.
[30] L. W. Tutt, T. F. Boggess, *Prog. Quant. Electron.* **1993**, *17*, 299–338.
[31] A. Midya, V. Mamidala, J.-X. Yang, P. K. L. Ang, Z.-K. Chen, W. Ji, K. P. Loh, *Small* **2010**, *6*, 2292–2300.
[32] T. He, W. Wei, L. Ma, R. Chen, S. Wu, H. Zhang, L. Huang, G. G. Gurzadyan, H. Sun, unpublished results.

Received: November 1, 2011
Revised: February 13, 2012
Published online: April 20, 2012

